BBA - Molecular Basis of Disease 1869 (2023) 166760

Contents lists available at ScienceDirect

BBA - Molecular Basis of Disease

journal homepage: www.elsevier.com/locate/bbadis

AOX delays the onset of the lethal phenotype in a mouse model of *Uqcrh* (complex III) disease

Howard T. Jacobs [a,b,*,1], Marten Szibor [a,c,1], Birgit Rathkolb [d,e,f], Patricia da Silva-Buttkus [d], Juan Antonio Aguilar-Pimentel [d], Oana V. Amarie [d], Lore Becker [d], Julia Calzada-Wack [d], Nathalia Dragano [d], Lillian Garrett [d], Raffaele Gerlini [d], Sabine M. Hölter [d,g], Tanja Klein-Rodewald [d], Markus Kraiger [d], Stefanie Leuchtenberger [d], Susan Marschall [d], Manuela A. Östereicher [d], Kristina Pfannes [d], Adrián Sanz-Moreno [d], Claudia Seisenberger [d], Nadine Spielmann [d], Claudia Stoeger [d], Wolfgang Wurst [g,h,i], Helmut Fuchs [d], Martin Hrabě de Angelis [d,f,j,**,1], Valérie Gailus-Durner [d,1]

[a] *Faculty of Medicine and Health Technology, FI-33014 Tampere University, Finland*
[b] *Department of Environment and Genetics, La Trobe University, Melbourne, Victoria 3086, Australia*
[c] *Department of Cardiothoracic Surgery, Center for Sepsis Control and Care (CSCC), Jena University Hospital, Friedrich Schiller University of Jena, Am Klinikum 1, 07747 Jena, Germany*
[d] *Institute of Experimental Genetics, German Mouse Clinic, Helmholtz Zentrum München, German Research Center for Environmental Health (GmbH), Ingolstaedter Landstraße 1, 85764 Neuherberg, Germany*
[e] *Institute of Molecular Animal Breeding and Biotechnology, Gene Center, Ludwig-Maximilians-University München, Feodor-Lynen Str. 25, 81377 Munich, Germany*
[f] *German Center for Diabetes Research (DZD), Ingolstaedter Landstraße 1, 85764 Neuherberg, Germany*
[g] *Institute of Developmental Genetics, Helmholtz Zentrum München, German Research Center for Environmental Health, Ingolstaedter Landstrasse 1, 85764 Neuherberg, Germany*
[h] *Chair of Developmental Genetics, TUM School of Life Sciences, Technische Universität München, Freising-Weihenstephan, Germany*
[i] *Deutsches Institut für Neurodegenerative Erkrankungen (DZNE) Site Munich, Feodor-Lynen-Str. 17, 81377 Munich, Germany*
[j] *Chair of Experimental Genetics, TUM School of Life Sciences, Technische Universität München, Alte Akademie 8, 85354 Freising, Germany*

ARTICLE INFO

Keywords:
Mitochondrial disease
Complex III
Alternative oxidase
Hyperglycemia
Growth impairment
Insulin sensitivity

ABSTRACT

The alternative oxidase, AOX, provides a by-pass of the cytochrome segment of the mitochondrial respiratory chain when the chain is unavailable. AOX is absent from mammals, but AOX from *Ciona intestinalis* is benign when expressed in mice. Although non-protonmotive, so does not contribute directly to ATP production, it has been shown to modify and in some cases rescue phenotypes of respiratory-chain disease models. Here we studied the effect of *C. intestinalis* AOX on mice engineered to express a disease-equivalent mutant of Uqcrh, encoding the hinge subunit of mitochondrial respiratory complex III, which results in a complex metabolic phenotype beginning at 4–5 weeks, rapidly progressing to lethality within a further 6–7 weeks. AOX expression delayed the onset of this phenotype by several weeks, but provided no long-term benefit. We discuss the significance of this finding in light of the known and hypothesized effects of AOX on metabolism, redox homeostasis, oxidative stress and cell signaling. Although not a panacea, the ability of AOX to mitigate disease onset and progression means it could be useful in treatment.

1. Introduction

Aerobic cellular respiration is made up of three key components: glycolysis, the Krebs cycle and oxidative phosphorylation (OXPHOS). The OXPHOS system comprises the mitochondrial respiratory chain (mRC), composed of four multi-subunit enzyme complexes (cI-cIV), plus

* Correspondence to: H. T. Jacobs, Faculty of Medicine and Health Technology, FI-33014 Tampere University, Finland.
** Correspondence to: M. Hrabě de Angelis, Institute of Experimental Genetics, German Mouse Clinic, Helmholtz Zentrum München, 85764 Neuherberg, Germany.
E-mail addresses: howard.jacobs@tuni.fi, howy@jacobs.net (H.T. Jacobs), hrabe@helmholtz-muenchen.de (M. Hrabě de Angelis).
[1] Who share senior authorship.

https://doi.org/10.1016/j.bbadis.2023.166760
Received 9 March 2023; Received in revised form 24 April 2023; Accepted 16 May 2023
Available online 23 May 2023

ATP synthase (complex V, cV). Together, they are responsible for ATP production, resulting from the release of free energy from the oxidation of carbohydrates, fats and other primary metabolites. Consequently, pathological dysfunction of the mRC results in broad physiological disturbances affecting diverse organ systems.

The mRC comprises >70 different polypeptides, 13 of which are encoded in mitochondrial DNA (mtDNA). The system thus depends on a large apparatus of mtDNA maintenance and expression, as well as for protein import and assembly, functions encoded by hundreds of nuclear genes requiring tightly coordinated regulation. Mutations in any of them may result in mRC disease with complex phenotypes that remain poorly understood. For example, null mutations in the cIV assembly factor SURF1 result in one form of Leigh syndrome [1,2], a form of progressive CNS degeneration commencing in infancy [3]. Mutations in different genes contributing to mRC biosynthesis and maintenance, or even in the same gene, may produce diverse phenotypes of dramatically different severity and organ involvement [4,5]. For example, different mutations in the cI subunit NDUFB11 are associated with microphthalmia with linear skin defects, histiocytoid cardiomyopathy, sideroblastic anemia or hypertrophic cardiomyopathy combined with lactic acidosis [6–8]. A number of pathological mutations in both humans and mice, affecting different subunits of mRC complex III (cIII), have been described, including UQCRH, the subject of the present study [9].

We have previously proposed the alternative oxidase, AOX, as both a tool to investigate the molecular basis of mRC pathology and, in the longer term, as a possible therapy [10]. AOX, found in most eukaryotes, including plants and many animals, but not in insects or vertebrates [11], acts as a by-pass for the cytochrome segment of the mRC and buffers stresses resulting from mRC insufficiency [12,13]. The enzyme is non-protonmotive and hence thermogenic. However, due to its much lower effective affinity than cIII for its electron-donating substrate, ubiquinol, the reduced form of coenzyme Q (CoQ), AOX contributes to electron flow only when cIII and/or cIV are unavailable due to overload, damage or mutation, leading to ubiquinol accumulation. AOX thus minimizes the risk of over-accumulation of ubiquinol, to which has been attributed various damaging effects. Notably, these effects include the triggering of reverse electron transport (RET) through cI (Szibor et al, 2020), resulting in excess production of potentially harmful levels of reactive oxygen species (ROS), and the blockade of a host of metabolic reactions governed by cellular redox balance. Conversely, pathological outcomes resulting from an insufficiency of electron flow in the mRC upstream of cIII should not be alleviated by AOX.

To date, experiments on AOX using animal models of mitochondrial disorders have produced a number of seemingly discordant results, indicating that the underlying pathomechanisms in mRC disease are not straightforwardly predictable, and vary according to the tissue, mutational target, genetic background and environmental factors such as diet. Thus, although in both the fruit fly *Drosophila* [14] and in the mouse [15,16], ubiquitous AOX expression is essentially benign, effects in genetic, toxic and surgical disease models vary. Both flies and mice were rescued from the acute toxicity of respiratory poisons such as cyanide [14,15], which acts against cytochrome *c* oxidase (cIV) but not AOX. Substantial phenotypic rescue was also observed in flies where essential subunits of cIV (e.g., subunits VIa or VIIa) were knocked down by RNAi or were functionally impaired by point mutation [14,17]. However, null mutants or RNAi knockdown of core subunits were not rescued [14,17]. Mutations in components of the machineries of mitochondrial DNA maintenance or expression were generally not compensated by AOX [18,19], although phenotypic improvement was seen in one fly model of Parkinson's disease associated with a defect in the mtDNA polymerase [20] Conversely, fly models of neurodegenerative disease associated with oxidative [14] or proteotoxic [21] stress were clearly alleviated by AOX, though the exact mechanisms remain uncertain.

Implementation of AOX in mouse disease models has generated a similarly mixed picture. AOX produced a dramatic rescue of a mouse sepsis model based on LPS (lipopolysaccharide) injection [22], alleviated the lung pathology resulting from chronic exposure to toxic smoke [23] and prevented the most damaging effects of the disease-equivalent mutation in a cIII disease (GRACILE syndrome) model, involving the cIII assembly factor [24] Bcs1l. In contrast, in mouse models of cIV-deficient (*Cox15*-associated) skeletal myopathy [25], *Mcp1*-induced inflammatory cardiomyopathy [26] and cardiac ischemia/reperfusion [27], ubiquitous expression of AOX exacerbated pathological outcomes, which was hypothesized to result from the failure of repair and regeneration due to disrupted ROS signaling. AOX also abrogated hypoxia signaling in the lung [28]. One particularly puzzling observation is that, whereas AOX rescued the phenotype of the most affected organ in the *Bcs1l* (GRACILE syndrome) mutant model, the heart [24], it impacted the same organ negatively in other contexts [26,29].

To expand our understanding of how AOX modifies disease phenotypes associated with mRC dysfunction and thus reveal details of the underlying pathophysiology, we here studied its effects on a second cIII disease model. Mice bearing a deletion of most of the coding region of *Uqcrh* [9], encoding the 'hinge' subunit of cIII that has been suggested to bridge cytochrome c_1 to cytochrome *c* [30], manifest a failure to thrive, combined with a progressive metabolic phenotype characterized by disturbed glucose homeostasis, lactic acidosis and hyperammonemia, with onset around 5–6 weeks and death several weeks later. The *Uqcrh*$^{-/-}$ mouse phenotype shares some features with that of the *Bcs1l* (GRACILE syndrome) mutant [24,31], notably involving cardiac and kidney dysfunction, but also recalling the metabolic crisis seen in many cIII patients [32]. In addition, in the post growth-arrest phase there are widespread developmental abnormalities affecting most of the body's organ systems [9].

In the present study we bred mice to homozygosity for the *Uqcrh* deletion combined with hemizygosity for ubiquitously expressed AOX inserted at the *Rosa26* locus [16]. These mice are here designated as Uqox mice (see crossing scheme illustrated in Fig. S1A). They were compared with *Uqcrh* homozygous mutant littermates lacking AOX, here designated as Uqcrh mice, and with wild-type littermate animals in the same genetic background, C57BL/6NCrl (Fig. S1A). The Uqox mice initially had a much healthier appearance but, with a delay of approximately 3 weeks, eventually manifested a similar growth arrest and metabolic phenotype as the Uqcrh mice. A number of other physiological parameters showed modest improvements in the Uqox mice, when studied at the same age point, most likely reflecting this delay in the onset of symptomatic disease.

Although the gradual metabolic and physiological deterioration was not rescued permanently, we posit that AOX provides benefit in the immediate post-weaning period to mice deficient in cIII due to *Uqcrh* deletion.

2. Experimental procedures

2.1. Uqox mouse model generation

To test for possible rescue of the detrimental effects of the loss of Uqcrh protein in mice [9], we crossed the Uqcrh mouse line with AOX transgenic mice [16] that had previously been backcrossed for ≥7 generations from C57BL/6 J to C57BL/6NCrl background. For generating the mouse line to be analyzed, mice heterozygous for both the *Uqcrh* gene ablation [9] and AOX were crossed with Uqcrh heterozygotes lacking AOX, as illustrated in Fig. S1A. The mice resulting from this cross that were homozygous for the *Uqcrh* mutation and heterozygous for AOX are here designated as Uqox mice. The other genotypes of interest were homozygotes for the *Uqcrh* mutation (Uqcrh mice) and wild-type mice. Doubly heterozygous mice were used for maintenance breeding. Animals were ear-clipped at day 18–21 and left with their mother until weaning, as previously described [9,16]. After genotyping the cohort was separated by sex with 3 mice per cage, one wild-type, one Uqcrh and one Uqox.

2.2. Animal maintenance and ethical permits

Animals were maintained in IVC cages with water and standard mouse chow according to directive 2010/63/EU, German national laws and GMC housing conditions (www.mouseclinic.de). Uqcrh, Uqox and wild-type mice were fed ad libitum with moist food freshly supplied twice per day, in addition to the normal chow food. Animals were sacrificed at 9–12 weeks in accordance with ethical permits and standard protocols. All tests performed were approved by the responsible authority of the district government of Upper Bavaria.

2.3. Genotyping

Mice were genotyped as described previously [9,16].

2.4. Phenotyping

The experiments reported used three cohorts of animals. The first cohort, cohort I, comprised 41 females (15 wild-type, 16 Uqcrh and 10 Uqox) and 45 males (14 wild-type, 16 Uqcrh and 15 Uqox). The second, cohort II, comprised 45 males and 45 females, i.e., 15 animals of each sex and genotype. Cohort III consisted of 33 females (13 wild-type, 13 Uqcrh and 7 Uqox) and 30 males (9 wild-type, 12 Uqcrh and 9 Uqox). Results were obtained from these cohorts as indicated in figure legends and relevant tables, along with ages, sexes and numbers of animals analyzed. Phenotypic analyses were conducted according to published protocols [33] and as described previously [9,16,24], with relevant modifications as in figure legends, or as described below.

2.5. Body and organ weights

Body and organ weights were measured as previously described [9,33].

2.6. Clinical chemistry and hematology

Tail glucose was monitored periodically as described previously [34]. Terminal blood samples from non-fasted mice were taken by puncturing the retro-orbital plexus under isofluorane anesthesia, and processed as summarized in Fig. S1H, with implementation of the procedures indicated in the yellow boxes therein. Instruments used were Olympus AU480 for clinical chemistry and Sysmex XT-2000iV for hematology. Insulin, leptin, FGF21 and cytokine levels in plasma were determined with a combined electroluminescence multiplex assay system (Meso Scale Discovery, MSD, Rockville, MD, USA).

2.7. Dissections and histopathological analysis

Mouse tissues were dissected, paraffin-embedded, sectioned, stained conventionally with hematoxylin and eosin (H&E) and imaged with a NanoZoomer® 2.0-HT (Hamamatsu Photonics, Hamamatsu City, Japan) digital slide scanner as described previously [9]. Subcutaneous white (WAT) and brown adipose tissue (BAT) were collected, fixed by zinc-formalin immersion, paraffin-embedded and 3 μm sections were stained with H&E. Digital whole-slide images were acquired (x20) with the NanoZoomer® 2.0-HT digital slide scanner as above, for histomorphometric analysis.

2.8. WAT histomorphometric analysis

Six boxes (300 × 300 μm) were randomly positioned in each H&*E*-stained subcutaneous WAT image. Automatic adipocyte size and count analyses were performed using open-source software QuPath 0.3.0 [35]. Briefly, adipocyte detection was reliably performed using QuPath's cell detection algorithm function. In order to delete false-positive adipocyte assignments a random-forest classifier was trained. QuPath then automatically measured the distribution of areas per adipocyte for each box analyzed. Data was visualized by histograms or boxplots according to genotype, as presented in the figures.

2.9. Body composition analysis

Thoracic and pelvic adipose tissue mass were separately determined post mortem at 18 μm^3 voxel resolution using a SkyScan 1176 micro-CT system (Bruker microCT, Kontich, Belgium), using the following parameters: 50 kV source voltage, 500 μA source current, 240 ms exposure time, 360° rotation, 0.5° rotation step, 4 frame averages, 0.5 mm aluminum filter. Image reconstruction was performed using NRecon software (Bruker microCT, Kontich, Belgium; version 1.7.5). For reconstruction, symmetrical boxcar smoothing with a smoothing level of 10 was applied, together with 30 % beam hardening correction and a ring-artifact correction of 4. Contrast limits were set to achieve optimal soft tissue contrast, while saturating bone. From each whole-body dataset, the anatomical regions of the thorax and pelvis were extracted into two additional data files by using CTAn (CT analyzer software, Bruker microCT, Kontich, Belgium; version 1.20.8). The thoracic region was defined as the area from the cervical vertebra C1 to thoracic vertebra T12. The pelvic region covered the lumbar to sacral vertebrae L3 to S3. Adipose tissue volumetry was performed using a semi-automated tissue segmentation approach (3D Slicer, version 5.1 / r30987; www.slicer.org). Fat mass was estimated by assuming a fat density of 0.9 g/cm^3 [36]. Finally, total adipose tissue mass was defined as the sum of the thoracic and the pelvic fat masses determined, and divided by body-weight to extrapolate % adipose tissue for each mouse.

2.10. Energy metabolism analysis

Gas exchange (oxygen consumption and carbon dioxide production), heat production and substrate utilization were measured for individually caged mice by indirect calorimetry in metabolic home cages (TSE Systems GmbH, Berlin, Germany, see https://www.mousephenotype.org/impress/ProcedureInfo?action=list&procID=852&pipeID=7). The measurement commenced five hours before lights off and finished four hours after lights-on the next morning (21 h in total).

2.11. Infrared (IR) thermography

Whole-body surface temperature of unrestrained conscious mice was dorsally captured by IR thermography (A655sc, FLIR Systems), with ambient temperature set to 21–22 °C.

2.12. Cardiac and muscle performance

Cardiac parameters were estimated by transthoracic echocardiography (TTE) on conscious mice, as previously described [9,37]. Two- and four-paw grip strength was estimated as the mean of three consecutive trials of each mouse analyzed, as described previously [33].

2.13. Behavioral analyses

Behavior was evaluated using a modified SHIRPA protocol [33] as previously described [9]. Locomotor activity was measured in a viewing arena approximately 33 × 55 cm, with a grid of 11 cm squares drawn on the floor. Units of locomotor activity were defined as the number of squares crossed in the first 30 s after transfer of the animal into this arena, counted manually.

2.14. Statistical analyses

If not stated otherwise, data were analyzed using GraphPad Prism, LibreOffice Calc or R (version 3.24.34), applying ANOVA or by Wilcoxon rank-sum test as appropriate, and as indicated in figure legends.

Values of $p < 0.05$ were considered as significant, with no correction for multiple testing.

3. Results

3.1. Growth arrest and onset of metabolic phenotype are delayed by 3 weeks in Uqox mice

Although Uqcrh mice are close to normal weight 1–2 weeks postnatally, they stop growing after weaning and enter growth arrest by 5 weeks of age [9]. Uqox mice showed a similar growth arrest, although delayed by approximately 3 weeks (Fig. 1A, B). The body weight of Uqcrh mice at 8 weeks, i.e., 3 weeks after growth arrest had set in, was only 60–65 % that of wild-type controls (Fig. 1A, B, S1B, S1C, S1E, S1F). The body weight of Uqox mice at the same age was 80 % (females, Fig. 1A) and 88 % (males, Fig. 1B) of wild-type values, and 3 weeks after growth arrest (i.e., at 11 weeks) their body weight was approximately 73 % (females, Fig. 1A) or 80 % (males, Fig. 1B) that of wild-type littermates of the same age. Uqox, Uqcrh and wild-type mice were easily distinguishable visually at 10 weeks (Fig. 1C). In summary, Uqox mice displayed an overall healthier appearance than Uqcrh mice, but suffered a similar growth arrest with a delay of ~3 weeks.

In Uqcrh mice, growth arrest is accompanied by a progressive metabolic crisis and multi-organ dysfunction [9], requiring routine sacrifice at the age of 11 weeks. We measured a number of key blood parameters in parallel in Uqox, Uqcrh and wild-type mice (Fig. 2). Blood glucose after weaning was tracked in all genotypes until 9 weeks of age (Fig. 2A, Fig. 2B, S1D, S1G). At 4 weeks blood glucose was the same in all genotypes, but Uqcrh mice had become severely hyperglycemic by 6 weeks. Uqox also became hyperglycemic to the same degree, but with a delay of 3 weeks in females and 2 weeks in males (Fig. 2A-2C, S1D, SG). At the 9-week time point, Uqcrh but not Uqox mice also showed high insulin levels (Fig. 2D), indicating insulin resistance. Leptin levels were very low (Fig. 2E) in both Uqcrh and Uqox mice, whilst triglyceride (Fig. 2F) and lactate (Fig. 2G) were both elevated in Uqcrh mice, with little or no rescue in Uqox mice. Other plasma parameters, including markers for kidney and liver function (Fig. S2) fell into two broad categories: (i) some were clearly shifted towards wild-type values in Uqox

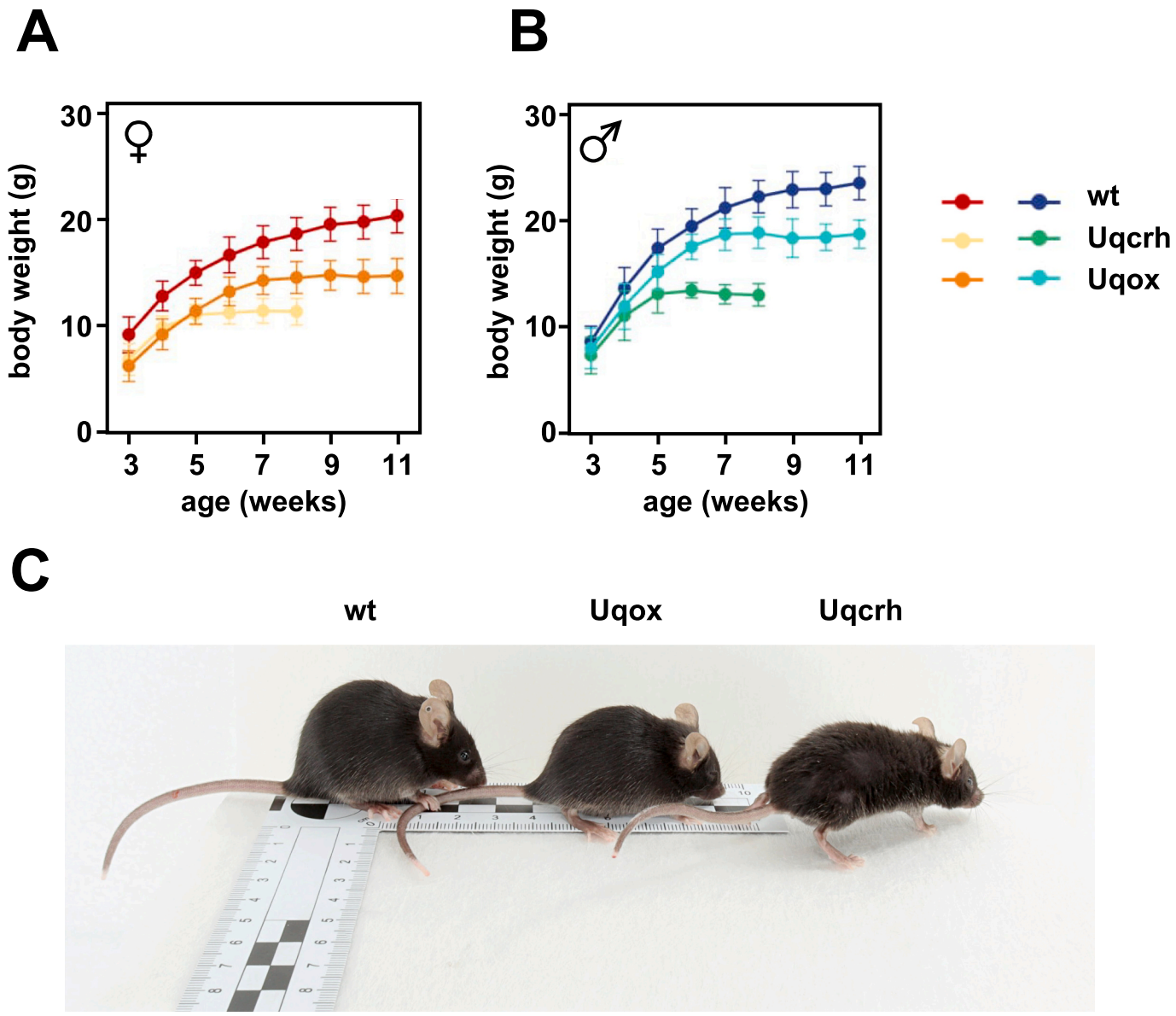

Fig. 1. Growth phenotype of Uqox mice
Body weight of (A) female and (B) male mice of the indicated genotypes (means ± SD) in the weeks after weaning. wt – wild-type. For cohort information and n numbers see Table S3. (C) Image of representative males of each genotype at 10 weeks. See also Fig. S1 for details of body weight changes.

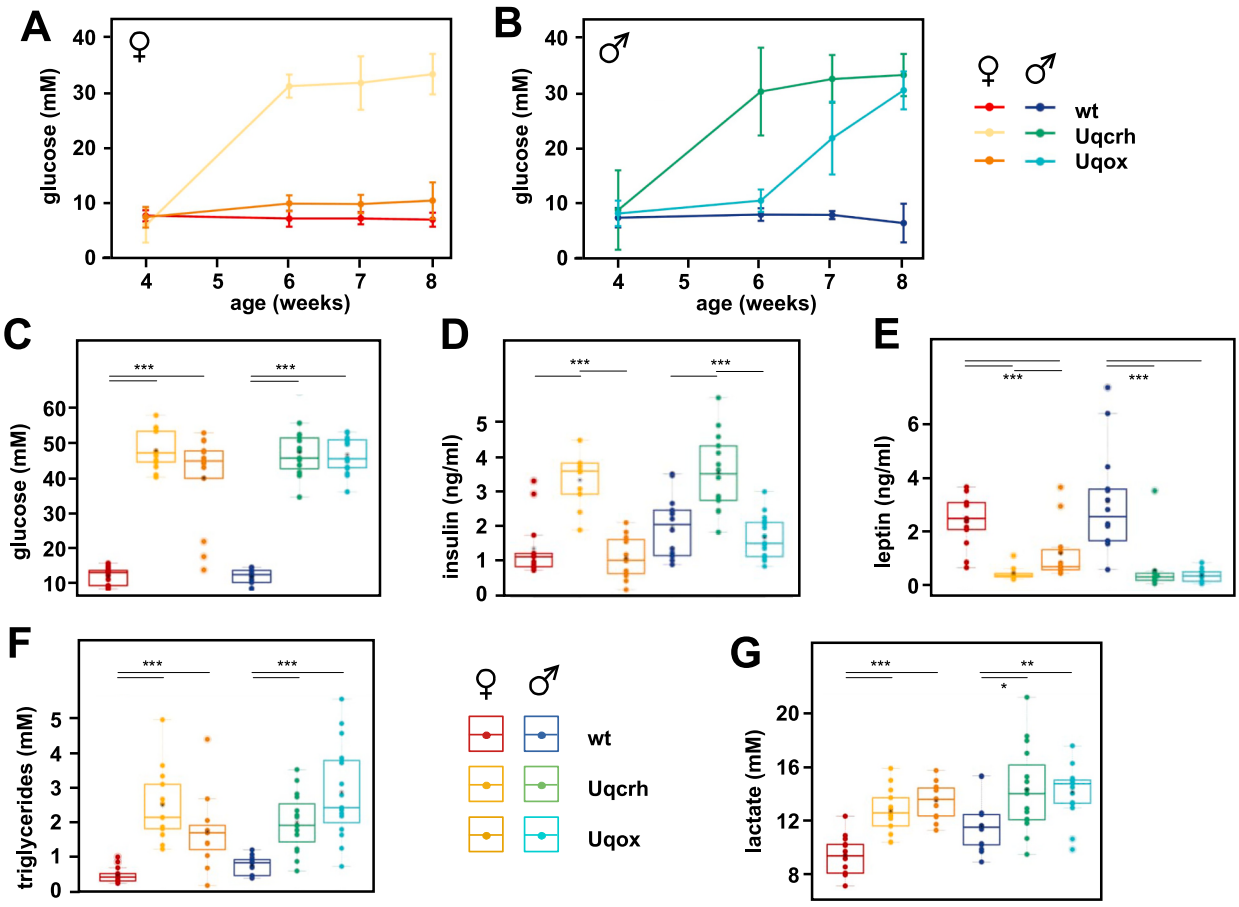

Fig. 2. Blood chemistry of Uqox mice

(A, B) Time course of blood glucose (tail-vein blood samples, means ± SD) in mice of the sex and genotype indicated. For statistical analysis of the week-on-week trends see Fig. S1B-G. (C-G) Plasma metabolites and hormones as shown, in 9-week old mice of the sex and genotype indicated (final clinical chemistry). Note that the mice were assayed and sacrificed unfasted, giving higher values for e.g. glucose or lactate than typical for fasted mice: see [38]. For cohort information and n numbers see Table S3. Boxplots follow standard Tukey convention (bars indicate median, 25th and 75th percentiles, whiskers at 1.5 IQR, ringed outliers beyond these limits, means denoted by faint asterisks). Statistical significance indicated by horizontal lines as per Table S1.

mice compared with Uqcrh, notably sodium (Fig. S2A), chloride (Fig. S2B), alkaline phosphatase (Fig. S2D), iron (Fig. S2E) and unsaturated iron-binding capacity (Fig. S2F); (ii) other markers that were abnormal in Uqcrh mice showed only minimal shifts towards normal physiological values in Uqox animals, namely inorganic phosphate (slightly elevated, Fig. S2C), total serum protein (slightly decreased, Fig. S2G), albumin (slightly decreased, Fig. S2H), lipase activity (low, Fig. S2I), urea (high, Fig. S2J), alanine aminotransferase (Fig. S2K) and aspartate aminotransferase (Fig. S2L), both slightly elevated. FGF21 levels showed only minor differences between the groups (Fig. S2M). Some pro-inflammatory cytokines that were elevated in Uqcrh mice were partially normalized in Uqox mice (IL-6, Fig. S2N), though for IL-2 only in males (Fig. S2O), whilst for IL-10 there was no such rescue (Fig. S2P). IL-5 was low in Uqcrh mice but restored in Uqox females and partially restored in Uqox males (Fig. S2Q). In summary, the metabolic phenotype manifested a few weeks later in Uqox compared to Uqcrh mice, with a minor sex difference in the delay to the onset of hyperglycemia. In addition, Uqcrh mice showed evidence suggestive of chronic inflammation, which was ameliorated in Uqox mice.

3.2. Key pathological markers are partially rescued in age-matched Uqox mice

In addition to growth arrest, Uqcrh mice show a number of features indicative of a multi-organ pathology, some of which were partly ameliorated in Uqox mice. Based on macroscopic examination upon dissection, the subcutaneous and perigonadal white adipose tissue (WAT) content of Uqcrh mice at 10 weeks appeared to be diminished compared with wild-type, but partially restored in Uqox animals (Fig. 3A, S3A). Histopathological examination of subcutaneous WAT tissue from wild-type mice showed uniform adipocytes containing single, large lipid droplets, with the nucleus pushed to the periphery of the cell (Fig. 3B, upper left panel, EV3B panel i). WAT from Uqcrh mice revealed adipocyte size alterations that appeared to be partially rescued in Uqox mice. Lipid droplets in Uqcrh WAT were microvesicular and appeared greatly diminished in size compared with wild-type, but shifted back towards wild-type size in Uqox animals at 10 weeks of age (Fig. 3B, upper panels, Fig. 3C, S3B panels i-iii). Histomorphometric WAT analysis (Fig. 3C, Fig. S3C) confirmed these findings. Interscapular brown adipose tissue (BAT) in wild-type mice presented small adipocytes with numerous small lipid droplets and an eccentrically located nucleus (Fig. 3C lower left panel, EV3B panel iv). In contrast, those in Uqcrh interscapular BAT were enlarged compared with wild-type, but appeared intermediate in Uqox animals (Fig. 3B, lower panels, Fig. S3B panels iv-vi).

Whereas in wild-type mice there was a clear distinction between white (WAT) and brown (BAT) intrascapular adipose tissue in the high-resolution CT data (Fig. S3D), Uqcrh and Uqox mice showed a more uniform X-ray absorption pattern in these fat depots (Fig. S3D). Consistent with this 'brightening' of brown fat in Uqcrh animals, body surface temperature showed a marked decline with age (Fig. 3D), commencing at 6–7 weeks, which was delayed by approximately 3

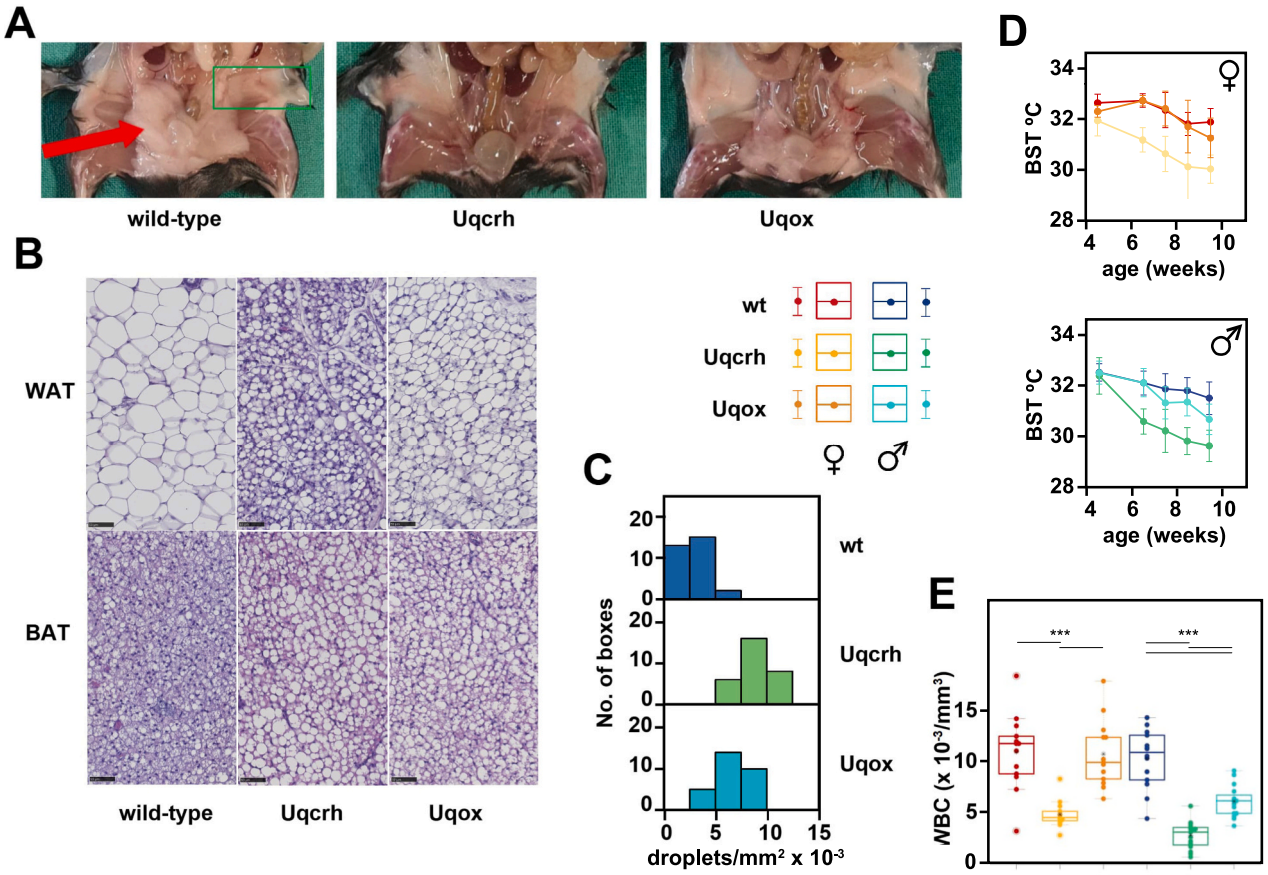

Fig. 3. Tissue phenotypes of Uqox mice

(A) Abdominal view of dissected, 10 week-old female mice of the indicated genotypes, showing perigonadal WAT (red arrow) and subcutaneous WAT (green box). For the corresponding whole-body images see Fig. S3A. (B) Representative micrographs of tissue sections from 10-week old male mice of the indicated genotype. WAT – white adipose tissue (here, subcutaneous), BAT – brown adipose tissue. Scale bars 100 μm. (C) Distribution of lipid droplet numbers from 10-week old male mice of the indicated genotype, $n = 5$ animals of each genotype, with six 300 × 300 μm boxes analyzed from sectioned, subcutaneous WAT of each mouse. Note that these are total counts across all boxes analyzed, not means. (D) Body surface temperature (BST) of mice of the indicated sex and genotype (means ± SD). (E) Leukocyte (WBC) counts as shown, for mice of the indicated sex and genotype, at 9 weeks. Statistical significance indicated by horizontal lines as per Table S1. For cohort information and n numbers see Table S3. Boxplot nomenclature as in Fig. 2.

weeks in Uqox animals (Fig. 3D). However, measurements of total fat mass as a proportion of body weight showed a clear deficit only in males, and this was not rescued in Uqox animals (Fig. S3E).

Hematological analysis of Uqcrh mice showed a very low leukocyte count (Fig. 3E), with an abnormally high proportion of leukocytes scored as neutrophils (Fig. S3F). In addition to macrocytosis (high MCV, Fig. S3G) and low mean corpuscular hemoglobin concentration (MCHC – Fig. S3H), platelet count was low (Fig. S3I). Uqox mice showed intermediate values for most of these markers (Fig. 3E, ES3F, S3H, S3I), though not MCV (Fig. S3G). Indirect calorimetry showed decreased rates of oxygen consumption and carbohydrate oxidation of Uqcrh mice at 9 weeks (Fig. S3J-S3M). The wild-type circadian pattern of fluctuation of both oxygen consumption (Fig. S3J, S3K) and carbohydrate oxidation (Fig. S3L, S3M) was absent in Uqcrh mice, similar to starvation conditions. Uqox mice of the same age showed a partial recovery in these parameters (Fig. S3J-S3M), especially in males (Fig. S3K, S3M), with the circadian pattern restored. Heat production corrected for body weight (Fig. S3N) showed no consistent trend, despite the morphological changes in BAT: the slight increase in Uqox males was not replicated in females.

Many of the internal organs of Uqcrh mice, when examined at 10 weeks, were disproportional when corrected for total body weight (Fig. S3O-S3R), and these abnormalities were at least partially rectified in Uqox animals, notably low heart (Fig. S3O), and spleen (Fig. S3P) weights, and high liver (Fig. S3Q, partially rescued only in Uqox females) and kidney (Fig. S3R) weights.

However, most histopathological features of the Uqcrh model were not convincingly ameliorated in Uqox animals examined at 10 weeks, including glycogen and/or fat deposits in the liver (red arrows, Fig. S3S), atrophic changes in the testis (Fig. S3T), ovary (Fig. S3U, red arrow denotes degenerating follicle – Foll; CL – corpus luteum) and thymus (Fig. S3V), and vacuolation in the myocardium (red arrows, Fig. S3W).

3.3. Functional abnormalities remain mainly unrescued in Uqox mice

We next conducted a series of tests of behavioral, cardiac and muscle function with a similar overall conclusion as from clinical chemistry and histopathology. On some key measures of behavior and muscle function, where Uqcrh mouse performance was poor, Uqox mice showed a partial functional rescue (Fig. 4). Other parameters showed only minimal, if any, improvement (Fig. S4). Thus, on a battery of behavioral tests conducted at 8 weeks, Uqox mice showed substantial amelioration on measures of locomotor activity (Fig. 4A) and tremor (Fig. 4B), but no major improvements in body position (Fig. S4A) transfer arousal (which was anyway only minimally affected in the mutant strain, Fig. S4B), or gait (Fig. S4C). Minor improvements in performance were more evident in males than females (Fig. S4A-S4C). Cardiac parameters were studied in Uqox versus control mice at 12 weeks, and compared with Uqcrh animals at 9 weeks. Cardiac measurements at a later time point were not possible in the Uqcrh mouse line, since this was the latest time point

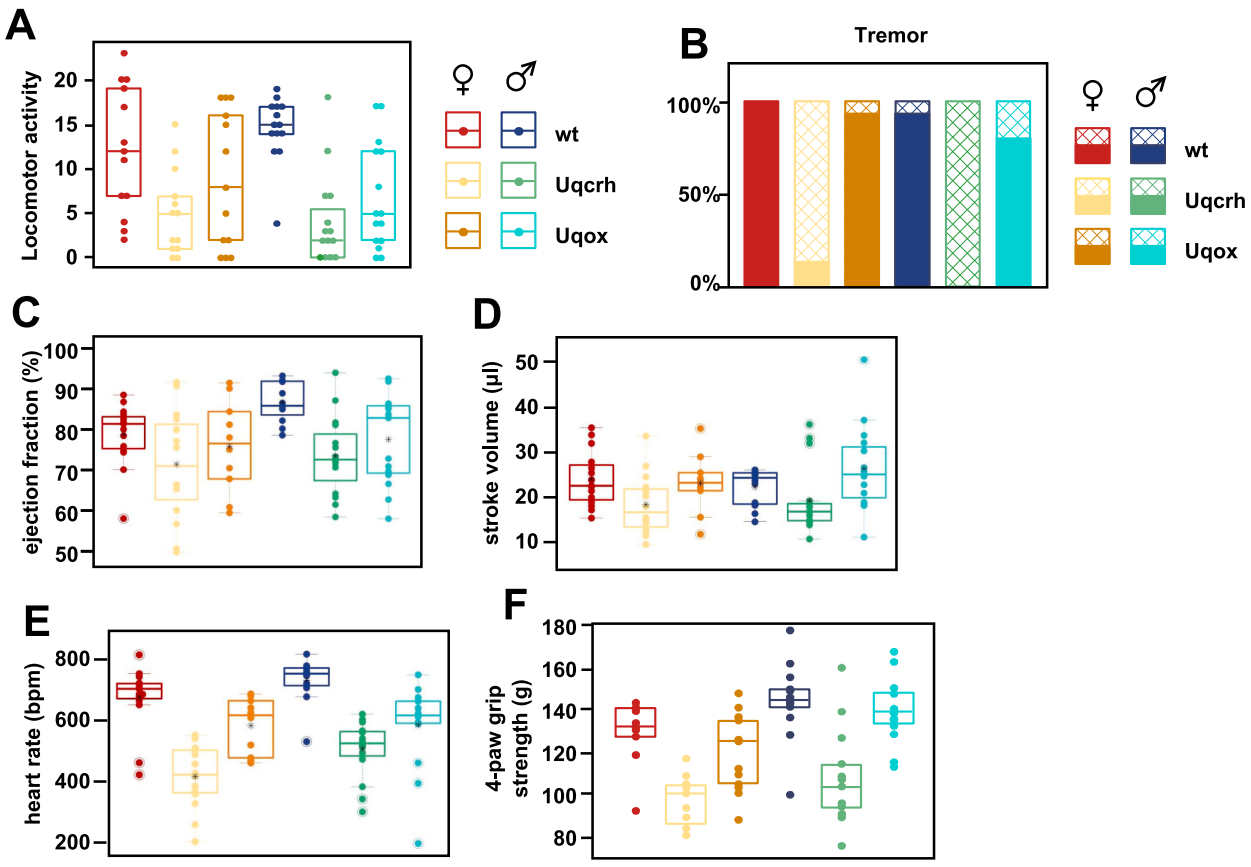

Fig. 4. Performance indicators of Uqox mice

(A) Locomotor activity of 8-week old mice of the indicated sex and genotype, units as defined in Materials and Methods. (B) Tremor scores (percentage of animals exhibiting tremor) from SHIRPA analysis of 8-week old mice of the sex and genotype indicated. Filled areas – tremor absent, cross-hatched areas – tremor present. (C, D, E) Cardiac parameters, as indicated, of mice of the indicated sex and genotype derived by echocardiography. Uqox and control mice were analyzed at 12 weeks, Uqcrh mice from the same cohort at 9 weeks. Parameters from Uqcrh mice of a separate cohort, measured alongside controls at 9 weeks, are shown here for comparison: see Table S2, which summarizes relevant data published elsewhere [34], bpm – beats per minute. *p*-values (Wilcoxon rank-sum test) for Uqox/wt comparison were as follows: ejection fraction, $p > 0.05$, females and $p < 0.05$, males; stroke volume $p > 0.5$, both sexes; heart rate, $p < 0.01$, females and $p < 0.001$, males. Note that full longitudinal characterization of cardiac phenotype of Uqcrh mutant mice will be published elsewhere. See also Fig. S4. (F) Mean 4-paw grip strength of 8-week old mice of the indicated sex and genotype (mean of 3 trials for each mouse studied). Statistical analyses (linear mixed effects model, S-plus) indicated significant effect of genotype (wt/Uqcrh: $p < 0.05$, Uqox/Uqcrh: $p < 0.05$) but also body-weight (wt/Uqcrh: $p < 0.001$, Uqox/Uqcrh: $p < 0.05$). For cohort information and n numbers see Table S3. Boxplot nomenclature as in Fig. 2. See also Fig. S4.

allowed by our ethical permit. Some cardiac parameters revealed partial or even complete functional normalization in the Uqox animals, notably ejection fraction (Fig. 4C), stroke volume (Fig. 4D) and heart rate (Fig. 4E) whilst some other parameters were apparently corrected to beyond wild-type values, such as left-ventricular (LV) inner cavity size (Fig. S4D) and mass (Fig. S4E). In terms of skeletal muscle function, grip strength (both 4-paw – Fig. 4F, and 2-paw – Fig. S4F) showed some improvement in Uqox compared with Uqcrh mice, when measured at 8 weeks, though statistical analysis revealed a confounding influence of body weight (see legends to Fig. 4F, S4F). Upon repeated trials many Uqcrh males, but not Uqox males, became visibly exhausted in this assay.

3.4. Partial rescue in Uqox mice is mostly a delay in phenotypic deterioration

To distinguish phenotypic parameters that were truly rescued (or part-rescued) in Uqox mice from those where deterioration was merely delayed, we looked again at a number of parameters in Uqox mice 2–3 weeks later than the time-points shown in the various figures thus far presented, and compared them with wild-type mice of the same age (note that Uqcrh animals had already been sacrificed by this point). As summarized in Figs. 5 and S5, some phenotypes showed the expected deterioration, but some did not, whilst others revealed only a slight decline. Taking account of the fact that comparability is not exact, since wild-type mice at 10–12 weeks differ from those at 8–9 weeks, the following conclusions can be drawn: neuromuscular phenotypes (locomotor activity – Fig. 5A, 4-paw grip strength – Fig. 5B and tremor – Fig. 5C) showed a marked deterioration in Uqox mice at 10 weeks compared with 8 weeks. Leukocyte count (Fig. 5D) also showed a further decrease in Uqox mice, although serum iron (Fig. S5A) and unsaturated iron binding capacity (Fig. S5B) did not show the changes seen in Uqcrh mice (Fig. S2E, S22F), that were suggestive of hemolysis. Uqox mice at 11–12 weeks also did not manifest the large increase in insulin levels (Fig. 5E) seen in Uqcrh mice at 9 weeks (Fig. 2D), despite hyperglycemia (Fig. 2C). Electrolyte levels (Fig. S5C, S5D) and alkaline phosphatase (Fig. S5E) in Uqox mice remained at similar levels as at 9 weeks. Indirect calorimetry indicated a further decline in metabolic activity of Uqox mice at 11 weeks, with the circadian fluctuations of both oxygen consumption (Fig. S5F) and carbohydrate oxidation (Fig. S5G) largely abolished, as was seen in Uqcrh mice already at 9 weeks (Fig. S3J-S3M).

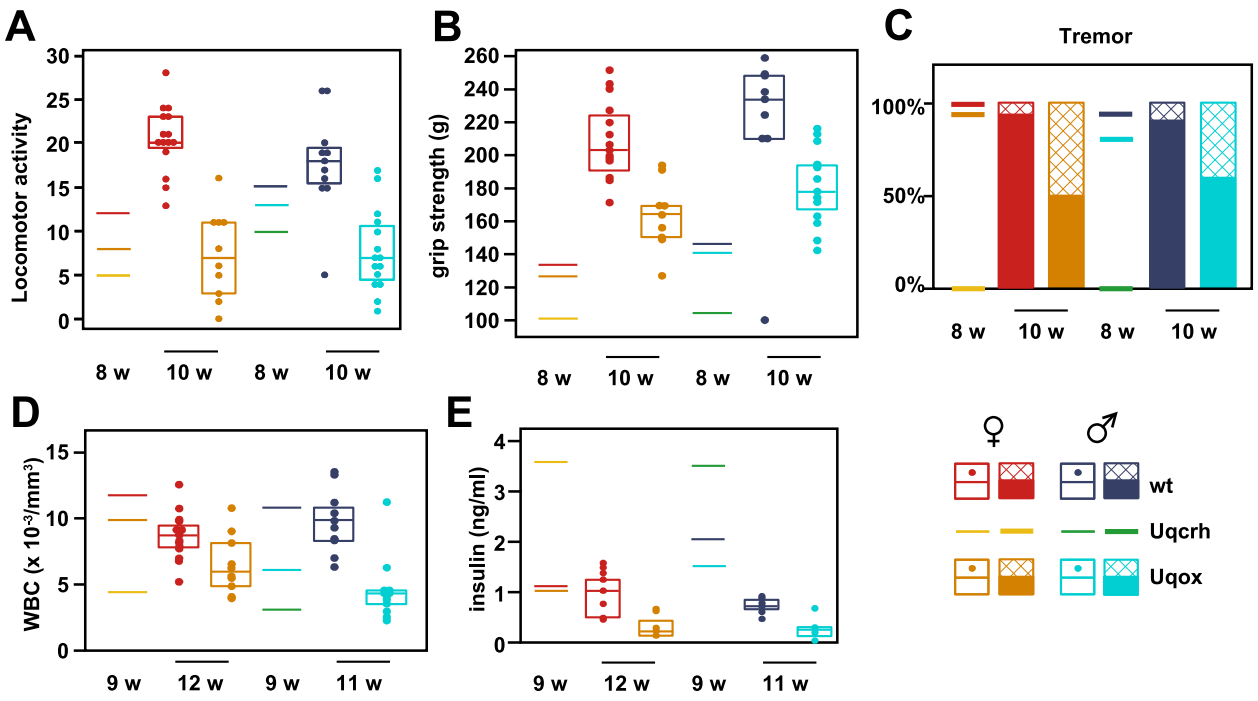

Fig. 5. Phenotypic indicators of late-stage Uqox mice
(A) Locomotor activity, (B) 4-paw grip strength, (C) tremor score, (D) leukocyte (WBC) count and (E) serum insulin of mice of the indicated ages, sexes and genotypes (nomenclature as for Fig. 2-4). For clarity, only the median values for mice at the earlier time points, reproduced from Figs. 2, 3 or 4 as appropriate, are shown. For cohort information and n numbers see Table S3. Note that Uqcrh mice had already been sacrificed (at 9 weeks) when the later assays were conducted.

4. Discussion

4.1. Overview

In this study we investigated the effect of expressing AOX, the alternative oxidase, in a mouse model of UQCRH (cIII) disease. Further details on the Uqcrh phenotype itself have been [34] or will be published elsewhere. Here we took advantage of the properties of AOX as a by-pass of the cytochrome segment of the mRC to obtain specific information concerning the pathomechanism behind the mutant phenotype. Ubiquitously expressed AOX [16] was able to delay the growth arrest and lethal metabolic crisis of the Uqcrh mouse, but only by ~3 weeks, with minor differences between the sexes. Many but not all pathological features of the model were mitigated by AOX expression, and are likely to be secondary to the metabolic disturbance and growth arrest. The metabolic phenotype in the Uqcrh mutant manifests at or very shortly after weaning, and is consistent with an inability to process carbohydrates and/or maintain glucose homeostasis. This is manifested as hyperglycemia and either by depletion of fat reserves or a failure in fat deposition, both processes being dependent on the functioning of the mRC [39] and shuttle systems [40]. The metabolic phenotype was accompanied by signs suggestive of starvation: low leptin levels, loss of the circadian pattern of metabolism, and thymic atrophy (consequent upon growth restriction), as also seen in *ob* homozygotes that lack endogenous leptin [41]. However, the 'starvation hormone' FGF21 [42,43], also diagnostic for some metabolic [44] and mitochondrial diseases [45], was not systematically induced by the *Uqcrh* mutation, with and without concomitant AOX expression.

Given the ~3 week delay produced by AOX, in the onset of the Uqcrh metabolic phenotype, the discussion of how AOX impacts the model has two, seemingly contradictory aspects: (i) why does AOX not rescue the model, even though it does modify and at least partially rescue other models of mRC disease and (ii) why does it nevertheless do so for a short time and to a limited extent. We now discuss these two aspects of our findings, and their possible meaning.

4.2. AOX non-rescue of the Uqcrh mouse model

The failure of AOX to effect a permanent rescue of the Uqcrh model is very unlikely to be due to low or insufficient expression. Hemizygous AOX expression from the Rosa26 locus was previously shown to be comparable at the protein, RNA and enzymatic level with that of endogenous OXPHOS-system genes and widespread across the tissues [16]. It was also sufficient to protect against LD50 doses of cyanide [16] and LPS [22] and to bring about a permanent rescue of the lethal cardiomyopathy of a second cIII disease model [24].

Since it was shown previously that expression of AOX in mouse heart results in a dramatic alleviation of H_2O_2 production when cIII is inhibited [16], its failure to prevent the lethal Uqcrh phenotype, effectively rargues against oxidative stress as an underlying pathological mechanism.

The simplest explanation for the essentially negative finding is that the Uqcrh pathology is due to a limitation on proton pumping at cIII and cIV, causing a deficiency of ATP production in one or more crucial tissues. In principle, AOX should be able to restore redox homeostasis and, by enabling unimpeded electron flow through cI, should at least partially restore mitochondrial ATP synthesis. However, this may be quantitatively insufficient to relieve the ATP deficiency and the metabolic response to it. Given that the instrumental tissue of any such effect is unknown, and may be a only very minor fraction of the whole animal by mass (e.g. part of an endocrine organ), or revealed only under specific physiological conditions (e.g. of nutrition, activity or circadian timing), it could easily escape detection.

Specific features of the Uqcrh phenotype suggest that other mechanisms may be involved. A failure to process carbohydrates implies that cells are starved of carbon skeletons for biosynthesis. AOX should facilitate forward electron flow through cI [27] and thus restore TCA cycle activity. However, this may depend on the functional partition of the quinone pool and the supercomplex organization of the respiratory membrane in different tissues and developmental stages [46,47], which has not yet been systematically studied even in wild-type mice.

Complexome analysis of heart mitochondria in Uqcrh mice found that cIII distribution in supercomplexes is abnormal, with almost no 'free' dimer detectable [9] and a very high molecular weight complex (denoted S_{XL}), containing cI, cIII and other polypeptides seen much more prominently [9]. Non-rescue by AOX may simply reflect the fact that AOX does not disturb supercomplex organization and does not directly interact with any of the individual OXPHOS complexes [15,16]. In previous work, cI activity in intact, proliferating cells grown in high glucose was shown to be shut down in response to cIII inhibition in a way that was not relieved by AOX [48]. Changes in supercomplex organization, for which cIII has been shown to play a crucial role [49], facilitate the switch between glycolysis and OXPHOS [50]. The absence of UQCRH may therefore block the switch to aerobic metabolism during development, and which is required for post-weaning growth. Intriguingly, a *Drosophila* mutant with mRC deficiency, manifesting a phenotype of growth impairment with sugar-intolerance and lactate overload [51], was also unmodified by the co-expression of AOX [18].

cIII dysfunction has been implicated in the induction of the tumor suppressor p53 in response to mRC inhibition [52], and *UQCRH* is the top-ranked gene down-regulated by hypermethylation in clear cell renal cell carcinoma [53,54]. UQCRH has been suggested to have a specific role in switching the cell's metabolic program between the glycolytic [55] and OXPHOS-based modes [56]. Although the mechanism of such a switch is not known, if it is unrelated to the redox function of cIII it would explain why AOX cannot alleviate its disruption.

UQCRH interacts with the Rieske iron-sulfur subunit and cytochrome *c*1 [57,58], as well as with cytochrome *c*. Its overexpression causes cytochrome *c* leakage into the cytosol, lowering the threshold for apoptosis [59]], whilst its silencing inhibits apoptosis [54]. Interference with the redox state of cytochrome *c* may disrupt apoptotic signaling [60], against which AOX would be ineffective.

4.3. Transient rescue of the Uqcrh model by AOX

There is little evidence of any correlation between the tissue pattern of AOX expression [16] and the degree or timing of rescue of the Uqcrh mutant phenotype by AOX. At the RNA level, AOX expression is highest in heart and skeletal muscle, lower in lung, liver, kidney and testis, and lowest in brain and spleen [16]. In terms of tissue pathology (Fig. S3S-S3W), there was no rescue in heart, liver or testis, and only a minimal rescue in thymus. Regarding relative organ sizes, there was an apparent rescue in heart (Fig. S3O) but only a partial rescue in spleen (Fig. S3P), liver (Fig. S3Q) and kidney (Fig. S3R), all to a similar extent. Functionally, the rescue in behavioral, cardiac and muscle parameters was partial (Fig. 4, S4) and/or transient (Fig. 5) in all cases. The tissue-specificity of the Uqcrh phenotype and the utility of AOX rescue could be explored further using conditional ablation of *Uqcrh*. This would first require generation of a conditional knock-out strain for the gene, which could then be combined with conditionally activatable AOX [26].

If a developmental switch in supercomplex organization in a specific tissue accounts for the failure of AOX to confer a permanent rescue, as suggested, the 3-week delay in the onset of the lethal phenotype may just reflect the time taken for the switch to take effect. The possible involvement of even larger assemblies involving components of the fatty acid oxidation pathway [61], the influence of various microproteins, of the pyruvate dehydrogenase complex and of the mitochondrial protease OMA1 in supercomplex architecture [50,62–64] should all be investigated further.

One intriguing difference between Uqcrh and Uqox mice is the fact that insulin levels are high in the former but remain low in the latter, even at 11–12 weeks when hyperglycemia is already well established and the mice are approaching the terminal state. Elevated insulin would be a logical response to hyperglycemia, except that it would have minimal physiological effect if the block on glucose utilization is far downstream. Mitochondrial OXPHOS is known to regulate insulin sensitivity [65]. The fact that AOX abolishes the elevation in insulin suggests that partial inhibition of cIII and/or cIV might be required for glucose sensing in the insulin-secreting cells of the pancreas. This recalls the finding that cIV inhibition is required for oxygen sensing, e.g., in pulmonary arterial smooth muscle cells, which is also relieved by AOX [28]. Although speculative, pancreatic overload of cIV by high glucose may generate a ROS signal, as hypothesized previously [80], that is required for insulin release. In the Uqox mouse, the alternative route for electron flow would abolish such a signal. Note, however, that no evidence for pancreatic dysfunction or impaired insulin release was seen in the AOX-expressing mouse in an otherwise wild-type background [16]. This may implicate cIII in the generation of such a signal, or could reflect a developmentally determined threshold effect.

4.4. Comparative effects of AOX in different cIII and cIV disease models

Knockout of mouse genes encoding core subunits of cIII such as Uqcrc1 [66] is lethal. However, three mouse models for cIII disease have now been created and characterized [9,67,68] that are not lethal in utero. Not only do they present differing degrees of phenotypic severity, but in the two that have been combined with AOX, different outcomes were observed. Knock-in of the GRACILE disease point mutation [69] to the gene encoding the cIII assembly factor Bcs1l produced distinct phenotypes when studied in two different mtDNA backgrounds, due to an otherwise sub-pathological mutation in the cytochrome *b* gene [31]. In the latter case, a phenotype at least as severe than that of Uqcrh was observed, with the mice suffering post-weaning growth arrest and death by 13 weeks, with a median lifespan of only ~5 weeks [68]. However, this background is apparently no longer available, and was not tested in combination with AOX. In a more wild-type mtDNA background, GRACILE mice survived until ~200 days, succumbing eventually to dilated cardiomyopathy and contractile failure [24,70]. AOX prevented cardiac and kidney pathology and produced a further lifespan extension to >500 days, in contrast to its inability to rescue the cardiac phenotype or lethal outcome in Uqcrh mice.

Intriguingly, tissue-specific ablation in catecholaminergic cells, of an essential cIII subunit, the Rieske iron-sulfur protein Uqcrfs1, produces a rather similar growth defect as observed here, which is associated with decreased levels of growth hormone [71]. There is no obvious explanation as to why AOX should fail to rescue this phenotype, unless the AOX transgene is not expressed in specific neuroendocrine cells. The issue could be explored further, for example by driving high-level AOX expression using the tyrosine hydroxylase promoter, as well as taking other mechanistic approaches to study why a neuroendocrine cIII defect impairs hormone secretion.

Transient or partial rescue by AOX in most cIII disease models contrasts with negative findings with cIV models. AOX had no impact on the early lethality of cardiomyocyte-specific *Cox10* knockout, nor on the cardiac insufficiency manifested in cardiomyocyte-specific *Cox10* heterozygotes [26]. Furthermore, the phenotype of skeletal muscle-specific *Cox15* knockout was exacerbated by AOX, by abrogating repair processes initiated by oxidative stress signaling [25]. AOX also provided no long-lasting benefit in mouse models of inflammatory cardiomyopathy [26] or cardiac ischemia-reperfusion [27], with cIV a major target, at least in the latter case.

Why cIII but not cIV deficiency in the heart was at least partially compensated by AOX remains to be explained. Note, however, that both of the cIII models tested retain residual function [9,24], whilst the cIV models involved the deletion of genes encoding enzymes needed for the biosynthesis of heme *a*, an essential prosthetic group of cIV [72], and are hence null mutants for cIV function. This may also impact supercomplex assembly [73].

Another possible explanation is that AOX cannot replace all of essential functions of the cytochrome chain. Although most flavin-linked dehydrogenases reduce ubiquinone, at least one, ALR (Evr1 in yeast), which serves as electron acceptor from Mia40 in the protein import and processing pathway to the mitochondrial intermembrane space, reduces

cytochrome *c* [74–77]. The yeast enzyme may also interact directly with oxygen [76,78]. AOX receives electrons directly from ubiquinol, serving as an alternative to cIII, but is unable to receive electrons from ALR/Evr1 in case of cIV deficiency.

4.5. Therapeutic potential of AOX

In contrast to initial hopes that AOX might be curative in cases of respiratory chain disease, whether in general [10] or, more specifically, in cases of cIII dysfunction [24], such a proposition now appears unrealistic. Although it is still not possible to account for the phenotypic diversity of mitochondrial disease itself, we now have to consider, in addition, the diversity of phenotypic effects conferred by AOX, at least in animal models, which can apparently vary from substantial rescue [14,17,21,24,79], through modest delay (as here), to no detectable effect at all [18,26], or even to exacerbation of disease phenotypes [25,26]. This does not mean that AOX might not be a useful therapeutic tool in some circumstances. However, any such application has to be based on a thorough exploration of its effects on mitochondrial metabolism and signaling in relevant contexts, and using reliable and valid models. In conclusion, whilst permanent rescue was not achieved, this study does provide novel insight into the functions of UQCRH and the nature of the physiological disturbances resulting from its absence.

Funding

The study was supported by the German Federal Ministry of Education and Research (Infrafrontier grant 01KX1012 to MHdA) and the German Center for Diabetes Research (DZD), also to MHdA. HTJ was supported in this work by grants from the European Research Council (232738) and Academy of Finland (283157 and 307431).

CrediT authorship contribution statement

Howard T. Jacobs: Conceptualization, methodology, formal analysis, writing (original draft), visualization, project administration, funding acquisition.

Marten Szibor: Conceptualization, methodology, writing (review and editing), supervision, project administration.

Birgit Rathkolb: Methodology, investigation, formal analysis, writing (review and editing), visualization.

Patricia da Silva-Buttkus: Methodology, investigation, formal analysis, writing (review and editing), visualization.

Juan Antonio Aguilar-Pimentel: Methodology, investigation, formal analysis, writing (review and editing), visualization.

Oana V. Amarie: Methodology, investigation, formal analysis, writing (review and editing), visualization.

Lore Becker: Methodology, investigation, formal analysis, writing (review and editing), visualization.

Julia Calzada-Wack: Methodology, investigation, formal analysis, writing (review and editing), visualization.

Nathalia Dragano: Methodology, investigation, formal analysis, writing (review and editing), visualization.

Lillian Garrett: Methodology, investigation, formal analysis, writing (review and editing), visualization.

Raffaele Gerlini: Methodology, investigation, formal analysis, writing (review and editing), visualization.

Sabine M. Hölter: Methodology, investigation, formal analysis, writing (review and editing), visualization.

Tanja Klein-Rodewald: Methodology, investigation, formal analysis, writing (review and editing), visualization.

Markus Kraiger: Methodology, investigation, formal analysis, writing (review and editing), visualization.

Stefanie Leuchtenberger: Methodology, investigation, formal analysis, writing (review and editing), visualization, supervision, project administration.

Susan Marschall: Methodology, investigation, formal analysis, writing (review and editing), visualization.

Manuela A. Östereicher: Methodology, investigation, formal analysis, writing (review and editing), visualization.

Kristina Pfannes: Methodology, investigation, formal analysis, writing (review and editing), visualization.

Adrián Sanz-Moreno: Methodology, investigation, formal analysis, writing (review and editing), visualization.

Claudia Seisenberger: Methodology, investigation, formal analysis, writing (review and editing), visualization,

Nadine Spielmann: Methodology, investigation, formal analysis, writing (review and editing), visualization.

Claudia Stoeger: Methodology, investigation, formal analysis, writing (review and editing), visualization.

Wolfgang Wurst: Conceptualization, methodology, writing (review and editing), supervisio, project administration.

Helmut Fuchs: Conceptualization, methodology, writing (review and editing), supervision, project administration, funding acquisition.

Martin Hrabě de Angelis: Conceptualization, methodology, writing (review and editing), supervision, project administration, funding acquisition.

Valérie Gailus-Durner: Conceptualization, methodology, writing (review and editing), supervision, project administration.

Declaration of competing interest

The authors declare that they have no conflicts of interest regarding the contents of this article. MSz is a shareholder in a spin-off company founded to develop AOX-based therapeutics.

Data availability

Data will be made available on request.

Acknowledgments

We thank Tea Tuomela for technical assistance and Aapo Kiviniemi for advice on legal matters.

Appendix A. Supplementary data

Supplementary data to this article can be found online at https://doi.org/10.1016/j.bbadis.2023.166760.

References

[1] V. Tiranti, K. Hoertnagel, R. Carrozzo, C. Galimberti, M. Munaro, M. Granatiero, L. Zelante, P. Gasparini, R. Marzella, M. Rocchi, et al., Mutations of SURF-1 in Leigh disease associated with cytochrome c oxidase deficiency, Am. J. Hum. Genet. 63 (1998) 1609–1621.

[2] Z. Zhu, J. Yao, T. Johns, K. Fu, I. De Bie, C. Macmillan, A.P. Cuthbert, R. F. Newbold, J. Wang, M. Chevrette, et al., SURF1, encoding a factor involved in the biogenesis of cytochrome c oxidase, is mutated in Leigh syndrome, Nat. Genet. 20 (1998) 337–343.

[3] A.Z. Lim, Y.S. Ng, A. Blain, C. Jiminez-Moreno, C.L. Alston, V. Nesbitt, L. Simmons, S. Santra, E. Wassmer, E.L. Blakely, et al., Natural history of Leigh syndrome: a study of disease burden and progression, Ann. Neurol. 91 (2022) 117–130.

[4] E. Fernandez-Vizarra, M. Zeviani, Mitochondrial disorders of the OXPHOS system, FEBS Lett. 595 (2021) 1062–1106.

[5] D. Orsucci, E. Caldarazzo Ienco, A. Rossi, G. Siciliano, M. Mancuso, Mitochondrial syndromes revisited, J Clin Med 10 (2021) 1249.

[6] D.A. Lichtenstein, A.W. Crispin, A.K. Sendamarai, D.R. Campagna, K. Schmitz-Abe, C.M. Sousa, M.D. Kafina, P.J. Schmidt, C.M. Niemeyer, J. Porter, et al., A recurring mutation in the respiratory complex 1 protein NDUFB11 is responsible for a novel form of X-linked sideroblastic anemia, Blood 128 (2016) 1913–1917.

[7] K. Reinson, R. Kovacs-Nagy, E. Õiglane-Shlik, S. Pajusalu, M. Nõukas, L.T. Wintjes, F.C.A. van den Brandt, M. Brink, T. Acker, U. Ahting, et al., Diverse phenotype in patients with complex I deficiency due to mutations in NDUFB11, Eur J Med Genet 62 (2019), 103572.

[8] A. Torraco, M. Bianchi, D. Verrigni, V. Gelmetti, L. Riley, M. Niceta, D. Martinelli, A. Montanari, Y. Guo, T. Rizza, D. Diodato, M. Di Nottia, et al., A novel mutation in

NDUFB11 unveils a new clinical phenotype associated with lactic acidosis and sideroblastic anemia, Clin Genet Mar 91 (3) (2017) 441–447.
[9] S. Vidali, R. Gerlini, K. Thompson, J.E. Urquhart, J. Meisterknecht, J.A. Aguilar-Pimentel, O.V. Amarie, L. Becker, C. Breen, J. Calzada-Wack, et al., Characterising a homozygous two-exon deletion in UQCRH: comparing human and mouse phenotypes, EMBO Mol Med 13 (2021), e14397.
[10] R. El-Khoury, K.K. Kemppainen, E. Dufour, M. Szibor, H.T. Jacobs, P. Rustin, Engineering the alternative oxidase gene to better understand and counteract mitochondrial defects: state of the art and perspectives, Br. J. Pharmacol. 171 (2014) 2243–2249.
[11] A.E. McDonald, G.C. Vanlerberghe, J.F. Staples, Alternative oxidase in animals: unique characteristics and taxonomic distribution, J. Exp. Biol. 212 (2009) 2627–2634.
[12] H.T. Jacobs, J.W.O. Ballard, What physiological role(s) does the alternative oxidase perform in animals? Biochim. Biophys. Acta Bioenerg. 1863 (2022), 148556.
[13] G.C. Vanlerberghe, Alternative oxidase: a mitochondrial respiratory pathway to maintain metabolic and signaling homeostasis during abiotic and biotic stress in plants, Int. J. Mol. Sci. 14 (2013) 6805–6847.
[14] D.J. Fernandez-Ayala, A. Sanz, S. Vartiainen, K.K. Kemppainen, M. Babusiak, E. Mustalahti, R. Costa, T. Tuomela, M. Zeviani, J. Chung, et al., Expression of the *Ciona intestinalis* alternative oxidase (AOX) in *Drosophila* complements defects in mitochondrial oxidative phosphorylation, Cell Metab. 9 (2009) 449–460.
[15] R. El-Khoury, E. Dufour, M. Rak, N. Ramanantsoa, N. Grandchamp, Z. Csaba, B. Duvillié, P. Bénit, J. Gallego, P. Gressens, et al., Alternative oxidase expression in the mouse enables bypassing cytochrome c oxidase blockade and limits mitochondrial ROS overproduction, PLoS Genet. 9 (2013), e1003182.
[16] M. Szibor, P.K. Dhandapani, E. Dufour, K.M. Holmström, Y. Zhuang, I. Salwig, I. Wittig, J. Heidler, Z. Gizatullina, T. Gainutdinov, et al., Broad AOX expression in a genetically tractable mouse model does not disturb normal physiology, Dis. Model. Mech. 10 (2017) 163–171.
[17] K.K. Kemppainen, J. Rinne, A. Sriram, M. Lakanmaa, A. Zeb, T. Tuomela, A. Popplestone, S. Singh, A. Sanz, P. Rustin, et al., Expression of alternative oxidase in Drosophila ameliorates diverse phenotypes due to cytochrome oxidase deficiency, Hum. Mol. Genet. 23 (2014) 2078–2093.
[18] K.K. Kemppainen, E. Kemppainen, H.T. Jacobs, The alternative oxidase AOX does not rescue the phenotype of *tko*^{25t} mutant flies, G3 (Bethesda) 420 (2014) 2013–2021.
[19] A.P.C. Rodrigues, A.F. Camargo, A. Andjelković, H.T. Jacobs, M.T. Oliveira, Developmental arrest in *Drosophila melanogaster* caused by mitochondrial DNA replication defects cannot be rescued by the alternative oxidase, Sci. Rep. 8 (2018) 10882.
[20] D.M. Humphrey, R.B. Parsons, Z.N. Ludlow, T. Riemensperger, G. Esposito, P. Verstreken, H.T. Jacobs, S. Birman, F. Hirth, Alternative oxidase rescues mitochondria-mediated dopaminergic cell loss in *Drosophila*, Hum. Mol. Genet. 21 (2012) 2698–2712.
[21] R. El-Khoury, E. Kaulio, K.A. Lassila, D.C. Crowther, H.T. Jacobs, P. Rustin, Expression of the alternative oxidase mitigates beta-amyloid production and toxicity in model systems, Free Radic. Biol. Med. 96 (2016) 57–66.
[22] E.L. Mills, B. Kelly, A. Logan, A.S.H. Costa, M. Varma, C.E. Bryant, P. Tourlomousis, J.H.M. Däbritz, E. Gottlieb, I. Latorre, et al., Succinate dehydrogenase supports metabolic repurposing of mitochondria to drive inflammatory macrophages, Cell 167 (2016) 457–470.e13.
[23] L. Giordano, A. Farnham, P.K. Dhandapani, L. Salminen, J. Bhaskaran, R. Voswinckel, P. Rauschkolb, S. Scheibe, N. Sommer, C. Beisswenger, et al., Alternative oxidase attenuates cigarette smoke-induced lung dysfunction and tissue damage, Am. J. Respir. Cell Mol. Biol. 60 (2019) 515–522.
[24] J. Rajendran, J. Purhonen, S. Tegelberg, O.P. Smolander, M. Mörgelin, J. Rozman, V. Gailus-Durner, H. Fuchs, M. Hrabe de Angelis, P. Auvinen, et al., Alternative oxidase-mediated respiration prevents lethal mitochondrial cardiomyopathy, EMBO Mol Med 11 (2019), e9456.
[25] S.A. Dogan, R. Cerutti, C. Benincá, G. Brea-Calvo, H.T. Jacobs, M. Zeviani, M. Szibor, C. Viscomi, Perturbed redox signaling exacerbates a mitochondrial myopathy, Cell Metab. 28 (2018) 764–775.e5.
[26] P.K. Dhandapani, I.M. Begines-Moreno, G. Brea-Calvo, U. Gärtner, T.G. Graeber, G. Javier Sanchez, R.E. Morty, K. Schönig, J.T. Hoeve, A. Wietelmann, et al., Hyperoxia but not AOX expression mitigates pathological cardiac remodeling in a mouse model of inflammatory cardiomyopathy, Sci. Rep. 9 (2019) 12741.
[27] M. Szibor, T. Gainutdinov, E. Fernandez-Vizarra, E. Dufour, Z. Gizatullina, G. Debska-Vielhaber, J. Heidler, I. Wittig, C. Viscomi, F. Gellerich, et al., Bioenergetic consequences from xenotopic expression of a tunicate AOX in mouse mitochondria: switch from RET and ROS to FET, Biochim. Biophys. Acta Bioenerg. 1861 (2020), 148137.
[28] N. Sommer, N. Alebrahimdehkordi, O. Pak, F. Knoepp, I. Strielkov, S. Scheibe, E. Dufour, A. Andjelković, A. Sydykov, A. Saraji, et al., Bypassing mitochondrial complex III using alternative oxidase inhibits acute pulmonary oxygen sensing, Sci. Adv. 6 (2020) eaba0694.
[29] M. Szibor, R. Schreckenberg, Z. Gizatullina, E. Dufour, M. Wiesnet, P. K. Dhandapani, G. Debska-Vielhaber, J. Heidler, I. Wittig, T.A. Nyman, et al., Respiratory chain signalling is essential for adaptive remodelling following cardiac ischaemia, J. Cell. Mol. Med. 24 (2020) 3534–3548.
[30] S. Ohta, K. Goto, H. Arai, Y. Kagawa, An extremely acidic amino-terminal presequence of the precursor for the human mitochondrial hinge protein, FEBS Lett. 226 (1987) 171–175.
[31] J. Purhonen, V. Grigorjev, R. Ekiert, N. Aho, J. Rajendran, R. Pietras, K. Truvé, M. Wikström, V. Sharma, A. Osyczka, et al., A spontaneous mitonuclear epistasis converging on Rieske Fe-S protein exacerbates complex III deficiency in mice, Nat. Commun. 11 (2020) 322.
[32] E. Fernández-Vizarra, M. Zeviani, Nuclear gene mutations as the cause of mitochondrial complex III deficiency, Front. Genet. 6 (2015) 13.
[33] H. Fuchs, V. Gailus-Durner, T. Adler, J.A. Aguilar-Pimentel, L. Becker, J. Calzada-Wack, P. Da Silva-Buttkus, F. Neff, A. Götz, W. Hans, et al., Mouse phenotyping, Methods 53 (2011) 120–135.
[34] N. Spielmann, C. Schenkl, T. Komlódi, P. da Silva-Buttkus, E. Heyne, J. Rohde, O. V. Amarie, B. Rathkolb, E. Gnaiger, T. Doenst, et al., Knockout of the complex III subunit Uqcrh causes bioenergetic impairment and cardiac contractile dysfunction, Mamm Genome (in press). (2022), https://doi.org/10.1007/s00335-022-09973-w. Epub ahead of print.
[35] P. Bankhead, M.B. Loughrey, J.A. Fernández, Y. Dombrowski, D.G. McArt, P. D. Dunne, S. McQuaid, R.T. Gray, L.J. Murray, H.G. Coleman, et al., QuPath: open source software for digital pathology image analysis, Sci. Rep. 7 (2017) 16878.
[36] T. Abe, R.S. Thiebaud, J.P. Loenneke, The mysterious values of adipose tissue density and fat content in infants: MRI-measured body composition studies, Pediatr. Res. 90 (2021) 963–965.
[37] K. Moreth, R. Fischer, H. Fuchs, V. Gailus-Durner, W. Wurst, H.A. Katus, R. Bekeredjian, M. Hrabě de Angelis, High-throughput phenotypic assessment of cardiac physiology in four commonly used inbred mouse strains, J. Comp. Physiol. B. 184 (2014) 763–775.
[38] T.L. Jensen, M.K. Kiersgaard, D.B. Sørensen, L.F. Mikkelsen, Fasting of mice: a review, Lab. Anim. 47 (2013) 225–240, https://doi.org/10.1177/0023677213501659.
[39] I.Y. Benador, M. Veliova, K. Mahdaviani, A. Petcherski, J.D. Wikstrom, E.A. Assali, R. Acín-Pérez, M. Shum, M.F. Oliveira, S. Cinti, et al., Mitochondria bound to lipid droplets have unique bioenergetics, composition, and dynamics that support lipid droplet expansion, Cell Metab. 27 (2018) 869–885.e6.
[40] K. Korla, L. Vadlakonda, C.K. Mitra, Kinetic simulation of malate-aspartate and citrate-pyruvate shuttles in association with Krebs cycle, J. Biomol. Struct. Dyn. 33 (2015) 2390–2403.
[41] J.K. Howard, G.M. Lord, G. Matarese, S. Vendetti, M.A. Ghatei, M.A. Ritter, R. I. Lechler, S.R. Bloom, Leptin protects mice from starvation-induced lymphoid atrophy and increases thymic cellularity in *Ob/Ob* mice, J. Clin. Invest. 104 (1999) 1051–1059.
[42] T. Inagaki, P. Dutchak, G. Zhao, X. Ding, L. Gautron, V. Parameswara, Y. Li, R. Goetz, M. Mohammadi, V. Esser, et al., Endocrine regulation of the fasting response by PPARalpha-mediated induction of fibroblast growth factor 21, Cell Metab. 5 (2007) 415–425.
[43] T. Uebanso, Y. Taketani, H. Yamamoto, K. Amo, H. Ominami, H. Arai, Y. Takei, M. Masuda, A. Tanimura, N. Harada, et al., Paradoxical regulation of human FGF21 by both fasting and feeding signals: is FGF21 a nutritional adaptation factor? PLoS One 6 (2011), e22976.
[44] X. Zhang, D.C. Yeung, M. Karpisek, D. Stejskal, Z.G. Zhou, F. Liu, R.L. Wong, W. S. Chow, A.W. Tso, K.S. Lam, et al., Serum FGF21 levels are increased in obesity and are independently associated with the metabolic syndrome in humans, Diabetes 57 (2008) 1246–1253.
[45] H. Tyynismaa, C.J. Carroll, N. Raimundo, S. Ahola-Erkkilä, T. Wenz, H. Ruhanen, K. Guse, A. Hemminki, K.E. Peltola-Mjøsund, V. Tulkki, et al., Mitochondrial myopathy induces a starvation-like response, Hum. Mol. Genet. 19 (2010) 3948–3958.
[46] E. Calvo, S. Cogliati, P. Hernansanz-Agustín, M. Loureiro-López, A. Guarás, R. A. Casuso, F. García-Marqués, R. Acín-Pérez, Y. Martí-Mateos, J.C. Silla-Castro, et al., Functional role of respiratory supercomplexes in mice: SCAF1 relevance and segmentation of the Qpool, Sci. Adv. 6 (2020) eaba7509.
[47] I. Vercellino, L.A. Sazanov, The assembly, regulation and function of the mitochondrial respiratory chain, Nat Rev Mol Cell Biol 23 (2022) 141–161.
[48] G. Cannino, R. El-Khoury, M. Pirinen, B. Hutz, P. Rustin, H.T. Jacobs, E. Dufour, Glucose modulates respiratory complex I activity in response to acute mitochondrial dysfunction, J. Biol. Chem. 287 (2012) 38729–38740.
[49] M. Protasoni, R. Pérez-Pérez, T. Lobo-Jarne, M.E. Harbour, S. Ding, A. Peñas, F. Diaz, C.T. Moraes, I.M. Fearnley, M. Zeviani, et al., Respiratory supercomplexes act as a platform for complex III-mediated maturation of human mitochondrial complexes I and IV, EMBO J. 39 (2020), e102817.
[50] E. Fernández-Vizarra, S. López-Calcerrada, A. Sierra-Magro, R. Pérez-Pérez, L. E. Formosa, D.H. Hock, M. Illescas, A. Peñas, M. Brischigliaro, S. Ding, et al., Two independent respiratory chains adapt OXPHOS performance to glycolytic switch, Cell Metab. 34 (2022) 1792–1808.e6.
[51] E. Kemppainen, J. George, G. Garipler, T. Tuomela, E. Kiviranta, T. Soga, C. D. Dunn, H.T. Jacobs, Mitochondrial dysfunction plus high-sugar diet provokes a metabolic crisis that inhibits growth, PLoS One 11 (2016), e0145836.
[52] A.A. Khutornenko, V.V. Roudko, B.V. Chernyak, A.B. Vartapetian, P.M. Chumakov, A.G. Evstafieva, Pyrimidine biosynthesis links mitochondrial respiration to the p53 pathway, Proc. Natl. Acad. Sci. U. S. A. 107 (2010) 12828–12833.
[53] Cancer Genome Atlas Research Network, Comprehensive molecular characterization of clear cell renal cell carcinoma, Nature 499 (2013) 43–49.
[54] K. Miyakuni, J. Nishida, D. Koinuma, G. Nagae, H. Aburatani, K. Miyazono, S. Ehata, Genome-wide analysis of DNA methylation identifies the apoptosis-related gene UQCRH as a tumor suppressor in renal cancer, Mol. Oncol. 16 (2022) 732–749.
[55] P. Vaupel, H. Schmidberger, A. Mayer, The Warburg effect: essential part of metabolic reprogramming and central contributor to cancer progression, Int. J. Radiat. Biol. 95 (2019) 912–919.

[56] Y. Luo, L. Medina Bengtsson, X. Wang, T. Huang, G. Liu, S. Murphy, C. Wang, J. Koren 3rd, Z. Schafer, X. Lu, UQCRH downregulation promotes Warburg effect in renal cell carcinoma cells, Sci. Rep. 10 (2020) 15021.
[57] C. Hunte, J. Koepke, C. Lange, T. Rossmanith, H. Michel, Structure at 2.3 Å resolution of the cytochrome bc(1) complex from the yeast *Saccharomyces cerevisiae* co-crystallized with an antibody Fv fragment, Structure 8 (2000) 669–684.
[58] D. Xia, C.A. Yu, H. Kim, J.Z. Xia, A.M. Kachurin, L. Zhang, L. Yu, J. Deisenhofer, Crystal structure of the cytochrome bc1 complex from bovine heart mitochondria, Science 277 (1997) 60–66.
[59] M. Okazaki, Y. Ishibashi, S. Asoh, S. Ohta, Overexpressed mitochondrial hinge protein, a cytochrome *c*-binding protein, accelerates apoptosis by enhancing the release of cytochrome *c* from mitochondria, Biochem. Biophys. Res. Commun. 243 (1998) 131–136.
[60] G.C. Brown, V. Borutaite, Regulation of apoptosis by the redox state of cytochrome *c*, Biochim. Biophys. Acta 1777 (2008) 877–881.
[61] Y. Wang, J. Palmfeldt, N. Gregersen, A.M. Makhov, J.F. Conway, M. Wang, S. P. McCalley, S. Basu, H. Alharbi, C. St Croix, et al., Mitochondrial fatty acid oxidation and the electron transport chain comprise a multifunctional mitochondrial protein complex, J. Biol. Chem. 294 (2019) 12380–12391.
[62] I. Bohovych, M.R. Fernandez, J.J. Rahn, K.D. Stackley, J.E. Bestman, A. Anandhan, R. Franco, S.M. Claypool, R.E. Lewis, S.S. Chan, et al., Metalloprotease OMA1 fine-tunes mitochondrial bioenergetic function and respiratory supercomplex stability, Sci. Rep. 5 (2015) 13989.
[63] C.A. Makarewich, A.Z. Munir, S. Bezprozvannaya, A.M. Gibson, S. Young Kim, M. S. Martin-Sandoval, T.P. Mathews, L.I. Szweda, R. Bassel-Duby, E.N. Olson, The cardiac-enriched microprotein mitolamban regulates mitochondrial respiratory complex assembly and function in mice, Proc. Natl. Acad. Sci. U. S. A. 119 (2022), e2120476119.
[64] C.S. Stein, P. Jadiya, X. Zhang, J.M. McLendon, G.M. Abouassaly, N.H. Witmer, E. J. Anderson, J.W. Elrod, R.L. Boudreau, Mitoregulin: a lncRNA-encoded microprotein that supports mitochondrial supercomplexes and respiratory efficiency, Cell Rep. 23 (2018) 3710–3720.e8.
[65] R.M. Morrow, M. Picard, O. Derbeneva, J. Leipzig, M.J. McManus, G. Gouspillou, S. Barbat-Artigas, C. Dos Santos, R.T. Hepple, D.G. Murdock, et al., Mitochondrial energy deficiency leads to hyperproliferation of skeletal muscle mitochondria and enhanced insulin sensitivity, Proc. Natl. Acad. Sci. U. S. A. 114 (2017) 2705–2710.
[66] W. Shan, J. Li, W. Xu, H. Li, Z. Zuo, Critical role of UQCRC1 in embryo survival, brain ischemic tolerance and normal cognition in mice, Cell. Mol. Life Sci. 76 (2019) 1381–1396.
[67] E. Bottani, R. Cerutti, M.E. Harbour, S. Ravaglia, S.A. Dogan, C. Giordano, I. M. Fearnley, G. D'Amati, C. Viscomi, E. Fernandez-Vizarra, et al., TTC19 plays a husbandry role on UQCRFS1 turnover in the biogenesis of mitochondrial respiratory complex III, Mol. Cell 67 (2017) 96–105.e4.
[68] P. Levéen, H. Kotarsky, M. Mörgelin, R. Karikoski, E. Elmér, V. Fellman, The GRACILE mutation introduced into *Bcs1l* causes postnatal complex III deficiency: a viable mouse model for mitochondrial hepatopathy, Hepatology 53 (2011) 437–447.
[69] I. Visapää, V. Fellman, J. Vesa, A. Dasvarma, J.L. Hutton, V. Kumar, G.S. Payne, M. Makarow, R. Van Coster, R.W. Taylor, et al., GRACILE syndrome, a lethal metabolic disorder with iron overload, is caused by a point mutation in *BCS1L*, Am. J. Hum. Genet. 71 (2002) 863–876.
[70] J. Purhonen, J. Rajendran, M. Mörgelin, K. Uusi-Rauva, S. Katayama, K. Krjutskov, E. Einarsdottir, V. Velagapudi, J. Kere, M. Jauhiainen, et al., Ketogenic diet attenuates hepatopathy in mouse model of respiratory chain complex III deficiency caused by a *Bcs1l* mutation, Sci. Rep. 7 (2017) 957.
[71] D. Cabello-Rivera, P. Ortega-Sáenz, L. Gao, A.M. Muñoz-Cabello, V. Bonilla-Henao, P.T. Schumacker, J. López-Barneo, Oxygen regulation of breathing is abolished in mitochondrial complex III-deficient arterial chemoreceptors, Proc. Natl. Acad. Sci. U.S.A. 119 (39) (2022 Sep 27).
[72] H.J. Kim, O. Khalimonchuk, P.M. Smith, D.R. Winge, Structure, function, and assembly of heme centers in mitochondrial respiratory complexes, Biochim. Biophys. Acta 1823 (2012) 1604–1616.
[73] F. Diaz, H. Fukui, S. Garcia, C.T. Moraes, Cytochrome *c* oxidase is required for the assembly/stability of respiratory complex I in mouse fibroblasts, Mol. Cell. Biol. 26 (2006) 4872–4881.
[74] S. Allen, V. Balabanidou, D.P. Sideris, T. Lisowsky, K. Tokatlidis, Erv1 mediates the Mia40-dependent protein import pathway and provides a functional link to the respiratory chain by shuttling electrons to cytochrome c, J. Mol. Biol. 353 (2005) 937–944.
[75] K. Bihlmaier, N. Mesecke, N. Terziyska, M. Bien, K. Hell, J.M. Herrmann, The disulfide relay system of mitochondria is connected to the respiratory chain, J. Cell Biol. 179 (2007) 389–395.
[76] D.V. Dabir, E.P. Leverich, S.K. Kim, F.D. Tsai, M. Hirasawa, D.B. Knaff, C. M. Koehler, A role for cytochrome *c* and cytochrome *c* peroxidase in electron shuttling from Erv1, EMBO J. 26 (2007) 4801–4811.
[77] S.R. Farrell, C. Thorpe, Augmenter of liver regeneration: a flavin-dependent sulfhydryl oxidase with cytochrome *c* reductase activity, Biochemistry 44 (2005) 1532–1541.
[78] X. Tang, S.K. Ang, E. Ceh-Pavia, D.J. Heyes, H. Lu, Kinetic characterisation of Erv1, a key component for protein import and folding in yeast mitochondria, FEBS J. 287 (2020) 1220–1231.
[79] A. Andjelković, K.K. Kemppainen, H.T. Jacobs, ligand-bound geneswitch causes developmental aberrations in *Drosophila* that are alleviated by the alternative oxidase, G3 (Bethesda) 6 (9) (2016) 2346–2839.
[80] J. Pi, Q. Zhang, J. Fu, C.G. Woods, Y. Hou, B.E. Corkey, S. Collins, M.E. Andersen, ROS signaling, oxidative stress and Nrf2 in pancreatic beta-cell function, Toxicol. Appl. Pharmacol. 244 (2010) 77–83.